Geomechanics and Engineering, *Vol. 35, No. 3 (2023) 255-270*
https://doi.org/10.12989/gae.2023.35.3.255

Pullout capacity analysis of an inclined shallow anchor plate embedded in sloping rock ground

Hong-tao Wang*[1,2], Fu-qiang Fan[1,3], Yan-qing Men[2], Hong-jun Zhang**[4] and Xue-lei Xie[1]

[1]*School of Civil Engineering, Shandong Jianzhu University, Jinan, Shandong, China*
[2]*Jinan Rail Transit Group Co., Ltd., Jinan, Shandong, China*
[3]*Shandong Jigang Environmental Protection New Materials Co., Ltd., Jinan, Shandong, China*
[4]*Shandong Geological Sci. Institute, Jinan, Shandong, China*

(*Received August 15, 2022, Revised October 7, 2023, Accepted October 9, 2023*)

Abstract. To calculate the pullout capacity of a shallow-buried inclined strip anchor plate in sloping rock ground, this paper constructed a curve uplift failure mechanism of rock mass above the anchor plate. In this mechanism, the plane strain hypothesis in elasto-plastic mechanics and the Hoek-Brown failure criterion were employed. Then, according to the upper bound method and variational principle, this paper deduced the analytical expressions for the rock failure surface equation and for the anchor plate's ultimate pullout capacity in the limit state. Further, based on an equivalent transformation method of Hoek-Brown failure criterion, this paper analyzed the influence laws of the embedment depth/width ratio, ground inclination, anchor plate inclination and generalized Hoek-Brown strength parameters on the anchor plate's ultimate pullout capacity and rock failure range. Finally, a series of numerical simulation for pullout failure processes of a strip anchor plate with six inclinations were carried out to verify the validity of the proposed theoretical method. The research work in this paper can provide some theoretical reference for design and construction of strip anchor plates in sloping rock ground.

Keywords: Hoek-Brown failure criterion; inclined anchor plate; sloping ground; pullout capacity; upper bound method

1. Introduction

As a foundation that can effectively provide pullout capacity, the anchor plate has been widely applied in electric power pylons, TV communication towers, high-rise structures, floating offshore oil wells and other structure foundations that bear uplift load. The anchor plate foundation has many advantages, such as its convenient installation, economy and practicability. According to the geometrical shape, anchor plates can be classified into strip anchor plates, rectangular anchor plates and circular anchor plates; according to the embedment mode, anchor plates can be classified into horizontal anchor plates, inclined anchor plates and vertical anchor plates. In practical engineering, how to reasonably determine the anchor plate's pullout capacity has always been a major concern of design and construction personnel.

Strip anchor plates are longer along the length direction. Therefore, according to the plane strain hypothesis in elasto-plastic mechanics, it can be reduced to a relatively simple two-dimensional problem for analysis and processing. Many researchers have carried out extensive research on such anchor plates. For example, Hu *et al*. (2021) and Perazzelli and Anagnostou (2017) employed the upper bound method to study the pullout capacity of the shallow-buried strip anchor plate and the geometrical shape of the failure surface, and systematically analyzed the influence laws of geomaterial properties on the pullout capacity. Wang *et al.* (2014) and Zhao *et al.* (2018) introduced the nonlinear failure criterion to establish the kinematic admissible velocity fields for failure of the shallow-buried horizontal strip anchor plates, and obtained the analytical solution for the ultimate pullout capacity through upper bound analysis. Han *et al*. (2016) and Rokonuzzaman and Sakai (2012) investigated the soil failure mechanism above the anchor plate in sand or clay by means of laboratory model tests and numerical simulation technique. Choudhary and Dash (2017) analyzed the influence laws of sand density and embedment depth on the bearing mechanism of vertical anchor plates through laboratory tests. Zhang *et al.* (2019) utilized the upper limit theorem and the nonlinear Mohr-Coulomb criterion, and studied the ultimate bearing capacity of anchor plate in heterogeneous soil. Zhao *et al.* (2020) analyzed the influence of soil heterogeneity and nonlinearity on the ultimate bearing capacity of shallow horizontal anchor plate considering soil heterogeneity. Ganesh (2020) studied the interaction between adjacent anchor plates and their vertical ultimate pulling forces in sandy soil. Hu *et al.* (2022) also conducted two three-dimensional failure mechanisms for horizontally embedded circular and rectangular anchor plates. Hu *et al.* (2020) conducted pullout model tests of anchor plates, and proposed the method for calculating the vertical ultimate pullout capacity of shallow anchor plates in sand. Cerfontaine *et al*. (2019), Hao *et al.* (2014) and

*Corresponding author, Ph.D.
E-mail: wanghongtao918@163.com
**Ph.D.
E-mail: sdjzytgc918@163.com

ISSN: 2005-307X (Print), 2092-6219 (Online)

Roy (2020) systematically studied the influence laws of physical and mechanical properties such as plate shape, embedment depth, rock or soil density, deformability and dilatancy on the pullout capacity of anchor plates. By using the finite element method of limit analysis, Bhattacharya and Kumar (2016), Kumar and Kouzer (2008) and Khatri and Kumar (2009) studied the pullout capacity of horizontal anchor plates in sand or clay. In most of the above researches, it was commonly assumed that the anchor plate was embedded horizontally in horizontal ground, but the influence of the ground inclination and the anchor plate inclination on the pullout capacity had received relatively little attention.

In practical engineering, many structures in mountains, hills and other rock ground inevitably need to be built on the slope; the anchor plate often needs to be inclined due to different load action directions. In this field, Hanna *et al*. (2015) studied the pullout capacity and failure mechanism of shallow-buried inclined strip anchor plates in sand through limit equilibrium analysis and laboratory tests. Bhattacharya (2016) employed a lower bound limit analysis method with finite elements, and obtained the pullout capacity of strip anchor plates in clayey sloping ground under undrained condition. Yang *et al.* (2020) carried out a series of uplift load tests for scaled strip anchor plate models, and analyzed the influence of the distance from the anchor to the slope and the angle of the slope on the pullout capacity of horizontal strip anchor plates in sandy sloping ground. However, it should be noted that the above research works only focused on the anchor plates in sand or clay; the pullout capacity of inclined anchor plates in sloping rock ground need to be further studied and discussed.

Based on the above research works, this paper focused on the pullout capacity analysis of inclined anchor plates in sloping rock ground. Specifically, this paper constructed an asymmetric curve failure mechanism of rock mass above the anchor plate, and employed the Hoek-Brown strength criterion to characterize the rock failure. Then, based on the upper bound method and variational extremum principle, this paper deduced the analytical expressions for the rock failure surface equation and for the anchor plate's ultimate pullout capacity in the limit state. The research work in this paper can provide some theoretical reference for design of inclined anchor plate foundations in sloping rock ground.

2. Hoek-Brown failure criterion

The Hoek-Brown failure criterion (Hoek and Broen 1997, Hoek and Marinos 2007, Hoek and Broen 2019, Zhu *et al.* 2013), a criterion for hard rock mass, was first put forward by Hoek and Brown in 1980. Over the past 40 years, the criterion has undergone five major modifications and improvements. Now, it can not only evaluate the strength of hard rock mass, but also analyze the mechanical properties of jointed rock mass or loose fractured rock mass; it has been widely used in failure and stability analysis of geotechnical and underground engineering. In the Mohr's plane, the Hoek-Brown failure criterion can be expressed by normal stress σ_n and shear stress τ_n as (Hoek and Broen 1997, Wang *et al.* 2019, Wang *et al*. 2021, Zhu *et al*. 2013)

$$\tau_n = A\sigma_c\left[\left(\sigma_n + \sigma_t\right)\sigma_c^{-1}\right]^B \tag{1}$$

where, A and B are empirical coefficients related to rock-mass properties, and their values range from 0 and 1; σ_n and τ_n are the normal stress and shear stress at the rock failure surface respectively; σ_c and σ_t are the uniaxial compressive strength and tensile strength of the rock mass respectively. This paper employs this criterion to investigate the uplift failure of inclined anchor plates in sloping ground.

3. Failure mechanism of an inclined anchor plate embedded in a rock slope

As shown in Fig. 1, a strip anchor plate with an inclination of α and a width of $2b$ is embedded in a rock slope, the inclination of the slope is β. Under the continuous action of uplift load P_u, the anchor plate needs to overcome the rock weight, rock shear strength and additional surface load q to move up. This will cause a certain range of failure to the rock mass above. Moreover, because both the ground surface and the anchor plate have a certain inclination, the thickness of the corresponding overlying rock at any point on the surface of the anchor plate also varies. This will further influence the rock failure range above the anchor plate to present some asymmetric failure characteristics. According to the asymmetry, this paper constructed a new curve failure mechanism, as shown in Fig. 1. Specifically, the equation for the rock failure surface on the right side above the anchor plate is $f_1(x)$, and the failure width at the ground surface is d_1; the equation for the rock failure surface on the left side is $f_2(x)$, and the failure width at the ground surface is d_2. Meanwhile, in order to facilitate analysis, this paper constructed the Cartesian coordinate system xoy by taking the center of the anchor plate's upper surface as the origin O, the anchor plate's inclined direction as the x axis, and the pullout load's action direction as the y axis, as shown in Fig. 1. The corresponding vertical embedment depth of the anchor plate's center O is H.

It should be noted that the asymmetric failure mechanism of the anchor plate shown in Fig. 1 is completely different from the symmetric failure mechanism in Reference (Wang *et al*. 2014, Zhao 2018). When both the ground surface and the anchor plate are horizontal, the failure mechanism in Fig. 1 can be reduced to the symmetric mechanism in Reference (Wang *et al*. 2014, Zhao 2018). Further, according to the upper bound theorem of limit analysis, this paper also made the following assumptions to analyze the uplift failure of the anchor plate:

a. The uplift failure of the inclined strip anchor plate is regarded as a plane strain problem;

b. The anchor plate is regarded as a shallow-buried rigid body whose geometric deformation can be negligible;

c. The rock mass above the anchor plate is regarded as an ideal rigid-plastic material, and its failure complies with

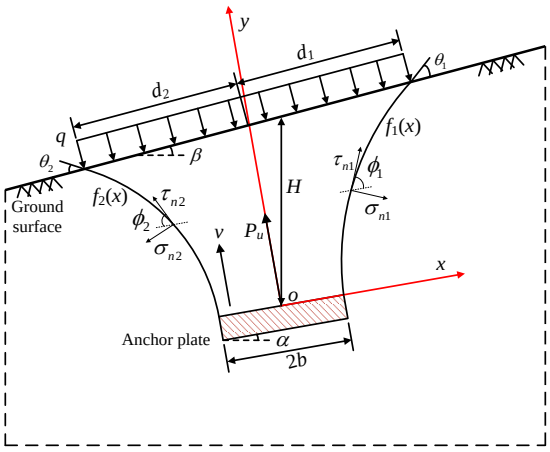

Fig. 1 Failure mechanism of an inclined strip anchor plate embedded in a slope

the Hoek-Brown failure criterion and its associated flow rule; the internal deformation of rock mass during the uplift failure process is ignored.

d. In the process of uplift failure, no relative sliding occurs between the anchor plate and the rock mass, and they both move upward with velocity v in the positive direction along the y axis.

Also notice that, in practical engineering, the ground excavation range above the anchor plate is often limited, and the excavation style can be stratified or partitioned due to installation process. Meanwhile, the filling material above the anchor plate can be concrete, cement mortar or other various types of materials. The installation process of anchor plate and the top filling material may significantly affect its bearing capacity. However, due to the complexity and diversity of the installation process of anchor plate, the influence of such factors was not incorporated into the theoretical failure mechanisms in most of existing research works and in this paper, which is also a limitation in current researches. In this paper, we just propose a theoretical prediction method for the pullout capacity of anchor plates in homogeneous Hoek-Brown medium, which can provide some theoretical guidance for anchor plate design practically.

4. Upper bound analysis on ultimate pullout capacity of an inclined anchor plate in a slope

According to the mechanism in Fig. 1 and the above assumptions, the internal energy dissipation rate and work rates of external forces corresponding to the uplift failure process of the anchor plate should be calculated first during the upper bound analysis. However, it should be noted that the failure mechanism in Fig. 1 shows obvious asymmetry; the rock failure range on the left side of the y axis and that on the right side of the y axis should be addressed separately. Taking the failure range on the right as an example, the rock failure surface can be regarded as a deformable thin layer based on the traditional plastic mechanics. The shear stress τ_n and normal stress σ_n at the thin layer satisfy the Hoek-Brown failure criterion expression in Eq. (1), and the corresponding rock yield function F can be expressed as

$$F = \tau_n - A\sigma_c\left[\left(\sigma_n + \sigma_t\right)\sigma_c^{-1}\right]^B \tag{2}$$

The plastic strain rate generated at the rock failure surface can be solved on the basis of the plastic potential theory (Chen 1975)

$$\dot{\varepsilon}_{ij} = \dot{\lambda}\frac{\partial Q}{\partial \sigma_{ij}} \tag{3}$$

where, Q is plastic potential function; $\dot{\lambda}$ is a plastic factor; $\dot{\varepsilon}_{ij}$ is plastic strain rate vector; σ_{ij} is stress vector.

If the Hoek-Brown yield function surface coincides with the plastic potential function surface in the principal stress space, we can establish an associated flow rule with the Hoek-Brown failure criterion. Then, set $Q = F$ and substitute Eq. (2) into Eq. (3); we may obtain the plastic strain rate at the rock failure surface on the right

$$\begin{cases} \dot{\varepsilon}_{n1} = \dot{\lambda}_1\dfrac{\partial \delta_1}{\partial \sigma_{n1}} = -\dot{\lambda}_1 AB\left[\left(\sigma_{n1} + \sigma_t\right)\sigma_c^{-1}\right]^{(B-1)} \\ \dot{\gamma}_{n1} = \dot{\lambda}_1\dfrac{\partial \delta_1}{\partial \tau_{n1}} = \dot{\lambda}_1 \end{cases} \tag{4}$$

where, $\dot{\varepsilon}_{n1}$ is plastic positive strain rate; $\dot{\gamma}_{n1}$ is plastic shear strain rate.

Meanwhile, according to the geometric relationships in Fig. 1, the plastic strain rate at the rock failure surface on the right can also be expressed by equation $f_1(x)$ as

$$\begin{cases} \dot{\varepsilon}_{n1} = \left(v / w_1\right)\left[1 + f_1'(x)^2\right]^{-1/2} \\ \dot{\gamma}_{n1} = -\left(v / w_1\right) f_1'(x)\left[1 + f_1'(x)^2\right]^{-1/2} \end{cases} \tag{5}$$

where, w_1 is the thickness of the thin layer at the rock failure surface on the right; $f_1'(x)$ is the first derivative of $f_1(x)$.

For the same failure mechanism, the plastic strain rate in Eq. (4) and that in Eq. (5) should be equivalent. Accordingly, we may set Eqs. (4) and (5) to be equal, and the normal stress at the rock failure surface on the right can be obtained as:

$$\sigma_{n1} = -\sigma_t + \sigma_c\left[ABf_1'(x)\right]^{1/(1-B)} \tag{6}$$

Then, by using Eqs. (1), (5) and (6), the energy dissipation rate per unit volume $\dot{D}_1$ at the thin layer of the right failure surface can be expressed as

$$\dot{D}_1 = \sigma_{n1}\dot{\varepsilon}_{n1} + \tau_{n1}\dot{\gamma}_{n1} = \left\{\frac{\left[\sigma_t - \sigma_c A^{1/(1-B)} B^{1/(1-B)} f_1'(x)^{1/(1-B)} \cdot \left(1 - B^{-1}\right)\right]}{\left[w_1\sqrt{1 + f_1'(x)^2}\right]}\right\} v \tag{7}$$

Similarly, we may obtain the energy dissipation rate per unit volume $\dot{D}_2$ at the thin layer of the left failure surface:

$$\dot{D}_2=\sigma_{n2}\dot{\varepsilon}_{n2}+\tau_{n2}\dot{\gamma}_{n2}= \left\langle \begin{Bmatrix} \sigma_t-\sigma_c A^{1/(1-B)}B^{1/(1-B)}\left[-f_2'(x)\right]^{1/(1-B)}\cdot \\ \left(1-B^{-1}\right) \end{Bmatrix} / \left[w_2\sqrt{1+f_2'(x)^2}\right] \right\rangle v \tag{8}$$

where, w_2 is the thickness of the thin layer at the rock failure surface on the left.

By integrating Eqs. (7) and (8) along the rock failure curve on the right and that on the left respectively, we may obtain the internal energy dissipation rate generated at the rock failure surface on the right and that on the left respectively

$$\dot{W}_{i1}=\int_0^{S_1}\dot{D}_1 w_1 ds=\int_b^{d_1\cos(\beta-\alpha)}\dot{D}_1 w_1\sqrt{1+f_1'(x)^2}dx= \int_b^{d_1\cos(\beta-\alpha)}\begin{bmatrix}\sigma_t-\sigma_c A^{1/(1-B)}B^{1/(1-B)}\cdot \\ f_1'(x)^{1/(1-B)}\cdot\left(1-B^{-1}\right)\end{bmatrix}dx\cdot v \tag{9}$$

$$\dot{W}_{i2}=\int_0^{S_2}\dot{D}_2 w_2 ds=\int_{-d_2\cos(\beta-\alpha)}^{-b}\dot{D}_2 w_2\sqrt{1+f_2'(x)^2}dx= \int_{-d_2\cos(\beta-\alpha)}^{-b}\begin{Bmatrix}\sigma_t-\sigma_c A^{1/(1-B)}B^{1/(1-B)} \\ \cdot\left[-f_2'(x)\right]^{1/(1-B)}\cdot\left(1-B^{-1}\right)\end{Bmatrix}dx\cdot v \tag{10}$$

where, S_1 is the total length of $f_1(x)$ in the interval $\left[b, d_1\cos(\beta-\alpha)\right]$; S_2 is the total length of $f_2(x)$ in the interval $\left[-d_2\cos(\beta-\alpha), -b\right]$.

By adding Eqs. (9) and (10), we may obtain the total internal energy dissipation rate $\dot{W}_i$ corresponding to the failure mechanism in Fig. 1

$$\dot{W}_i=\dot{W}_{i1}+\dot{W}_{i2}= \int_b^{d_1\cos(\beta-\alpha)}\begin{Bmatrix}\sigma_t-\sigma_c A^{1/(1-B)}B^{1/(1-B)}f_1'(x)^{1/(1-B)}\cdot \\ \left(1-B^{-1}\right)\end{Bmatrix}dx\cdot v+ \int_{-d_2\cos(\beta-\alpha)}^{-b}\begin{Bmatrix}\sigma_t-\sigma_c A^{1/(1-B)}B^{1/(1-B)}\left[-f_2'(x)\right]^{1/(1-B)} \\ \cdot\left(1-B^{-1}\right)\end{Bmatrix}dx\cdot v \tag{11}$$

In the failure mechanism shown in Fig. 1, during the action process of the uplift load, the inclined anchor plate needs to overcome the effect of the rock weight and ground surface load. The corresponding work rates of external forces include the work rate of rock weight, the work rate of ground surface load and the work rate of the anchor plate's ultimate pullout capacity. According to the geometric relationships in Fig. 1, we may obtain the work rate of rock weight on the right side above the anchor plate

$$\dot{W}_{\gamma 1}=-\left\{\begin{bmatrix}\dfrac{Hd_1\cos(\beta-\alpha)}{(1+\tan\alpha\cdot\tan\beta)\cos\alpha}+ \\ \dfrac{1}{4}d_1^2\sin 2(\beta-\alpha)\end{bmatrix}\gamma-\int_b^{d_1\cos(\beta-\alpha)}f_1(x)\gamma dx\right\}\cdot v\cos\alpha \tag{12}$$

where, γ is the unit weight of rock mass.

The work rate of rock weight on the left side above the anchor plate is

$$\dot{W}_{\gamma 2}=-\left\{\begin{bmatrix}\dfrac{Hd_2\cos(\beta-\alpha)}{(1+\tan\alpha\cdot\tan\beta)\cos\alpha}- \\ \dfrac{1}{4}d_2^2\sin 2(\beta-\alpha)\end{bmatrix}\gamma-\int_{-d_2\cos(\beta-\alpha)}^{-b}f_2(x)\gamma dx\right\}\cdot v\cos\alpha \tag{13}$$

By adding Eqs. (12) and (13), we may obtain the total work rate of rock weight above the anchor plate

$$\dot{W}_\gamma=\dot{W}_{\gamma 1}+\dot{W}_{\gamma 2}=-\left[\begin{bmatrix}\dfrac{H(d_1+d_2)\cos(\beta-\alpha)}{(1+\tan\alpha\cdot\tan\beta)\cos\alpha}+ \\ \dfrac{1}{4}\left(d_1^2-d_2^2\right)\sin 2(\beta-\alpha)\end{bmatrix}-\int_b^{d_1\cos(\beta-\alpha)}f_1(x)dx-\int_{-d_2\cos(\beta-\alpha)}^{-b}f_2(x)dx\right]\cdot\gamma v\cos\alpha \tag{14}$$

The work rate of the ground surface load is

$$\dot{W}_q=-qd_1 v\cos(\beta-\alpha)-qd_2 v\cos(\beta-\alpha)= -q(d_1+d_2)v\cos(\beta-\alpha) \tag{15}$$

where, q is ground surface load.

The work rate of the anchor plate's ultimate pullout capacity P_u is

$$\dot{W}_P=P_u\cdot v \tag{16}$$

On this basis, according to the principle of virtual work rate, set the total internal energy dissipation rate to be equal to the total work rates of external forces

$$\dot{W}_i=\dot{W}_P+\dot{W}_\gamma+\dot{W}_q \tag{17}$$

By substituting Eqs. (11), (14), (15) and (16) into Eq. (17) respectively, we may obtain the anchor plate's ultimate pullout capacity P_u after rearrangement

$$P_u=\begin{bmatrix}\dfrac{H(d_1+d_2)\cos(\beta-\alpha)}{(1+\tan\alpha\cdot\tan\beta)\cos\alpha}+ \\ \dfrac{1}{4}\left(d_1^2-d_2^2\right)\sin 2(\beta-\alpha)\end{bmatrix}\cdot\gamma\cos\alpha+ q(d_1+d_2)v\cos(\beta-\alpha)+ \int_b^{d_1\cos(\beta-\alpha)}\Lambda_1\left[f_1(x), f_1'(x), x\right]dx+ \int_{-d_2\cos(\beta-\alpha)}^{-b}\Lambda_2\left[f_2(x), f_2'(x), x\right]dx \tag{18}$$

where, $\Lambda_1\left[f_1(x), f_1'(x), x\right]$ and $\Lambda_2\left[f_2(x), f_2'(x), x\right]$ are functional of $f_1(x)$ and functional of $f_2(x)$ respectively.

Their expressions are as follows

$$\Lambda_1\left[f_1(x), f_1'(x), x\right]=\sigma_t-\sigma_c A^{1/(1-B)}\cdot B^{1/(1-B)}f_1'(x)^{1/(1-B)}\cdot\left(1-B^{-1}\right)-f_1(x)\gamma\cos\alpha \tag{19}$$

$$\Lambda_2\left[f_2(x), f_2'(x), x\right]=\sigma_t-\sigma_c A^{1/(1-B)}B^{1/(1-B)}\left[-f_2'(x)\right]^{1/(1-B)}\cdot\left(1-B^{-1}\right)-f_2(x)\gamma\cos\alpha \tag{20}$$

According to the upper bound theorem of the limit analysis theory, the failure load in Eq. (18) determined by the virtual work rate equation should be greater than or equal to the real ultimate pullout capacity of the anchor plate. That is, the minimum value of Eq. (18) in the corresponding integral interval should be sought if we want to obtain the ultimate pullout capacity that is closer to the real value. It should be noted that in Eq. (18), the minimum value of P_u mainly depends on $\Lambda_1\left[f_1(x), f_1'(x), x\right]$ and $\Lambda_2\left[f_2(x), f_2'(x), x\right]$ functionals. Furthermore, these are two simple integral-type functionals that can be solved by using the following Euler-Lagrange equations based on the variational principle.

$$\frac{\partial\Lambda_1}{\partial f_1(x)}-\frac{\partial}{\partial x}\left[\frac{\partial\Lambda_1}{\partial f_1'(x)}\right]=0 \tag{21}$$

$$\frac{\partial\Lambda_2}{\partial f_2(x)}-\frac{\partial}{\partial x}\left[\frac{\partial\Lambda_2}{\partial f_2'(x)}\right]=0 \tag{22}$$

By substituting Eqs. (19) and (20) into Eqs. (21) and (22) respectively, we may obtain the following equations

$$(B-1)^{-1}\sigma_c A^{1/(1-B)}B^{1/(1-B)}\cdot f_1''(x)^{(2B-1)/(1-B)}+\gamma\cos\alpha=0 \tag{23}$$

$$(B-1)^{-1}\sigma_c A^{1/(1-B)}B^{1/(1-B)}\cdot[-f_2''(x)]^{(2B-1)/(1-B)}+\gamma\cos\alpha=0 \tag{24}$$

Both Eqs. (23) and (24) are second-order homogeneous differential equations with constant coefficients. By integrating them twice separately, we may obtain

$$f_1(x)=\left(-\gamma\cos\alpha\right)^{-1}\sigma_c^{(B-1)/B}\cdot A^{-1/B}\left(M_1-\gamma\cos\alpha x\right)^{1/B}+N_1 \tag{25}$$

$$f_2(x)=-\sigma_c^{(B-1)/B}A^{-1/B}\left(\gamma\cos\alpha\right)^{-1}\cdot\left(M_2+\gamma\cos\alpha x\right)^{1/B}+N_2 \tag{26}$$

where, M_1, N_1, M_2 and N_2 are integration constants, which can be determined by the geometric boundary conditions in Fig. 1.

Specifically, according to the geometric relationships shown in Fig. 1, the rock failure curve $f_1(x)$ on the right should satisfy

$$f_1'(x)\Big|_{x=d_1\cos(\beta-\alpha)}=\tan\theta_1 \tag{27}$$

$$f_1(x)\Big|_{x=d_1\cos(\beta-\alpha)}=\frac{H}{\left(1+\tan\alpha\cdot\tan\beta\right)\cos\alpha}+d_1\sin\left(\beta-\alpha\right) \tag{28}$$

$$f_1(x)\Big|_{x=b}=0 \tag{29}$$

where, θ_1 is the angle between the rock failure curve . on the right side and the ground.

The rock failure curve $f_2(x)$ on the left should satisfy

$$f_2'(x)\Big|_{x=-d_2\cos(\beta-\alpha)}=-\tan\theta_2 \tag{30}$$

$$f_2(x)\Big|_{x=-d_2\cos(\beta-\alpha)}=\frac{H}{\left(1+\tan\alpha\cdot\tan\beta\right)\cos\alpha}-d_2\sin\left(\beta-\alpha\right) \tag{31}$$

$$f_2(x)\Big|_{x=-b}=0 \tag{32}$$

where, θ_2 is the angle between the rock failure curve $f_2(x)$ on the left side and the ground.

By substituting Eq. (25) into Eq. (27), we may obtain constant M_1

$$M_1=\tan^{B/(1-B)}\theta_1 A^{1/(1-B)}B^{B/(1-B)}\sigma_c+\gamma d_1\cos\alpha\cdot\cos\left(\beta-\alpha\right) \tag{33}$$

By substituting Eq. (25) into Eq. (27) and combining with Eq. (28), we may obtain constant N_1

$$N_1=\frac{H}{\left(1+\tan\alpha\cdot\tan\beta\right)\cos\alpha}+d_1\sin\left(\beta-\alpha\right)+\left(\gamma\cos\alpha\right)^{-1}\left[\tan^{1/(1-B)}\theta_1 A^{1/(1-B)}B^{1/(1-B)}\sigma_c\right] \tag{34}$$

By substituting Eq. (25) into Eq. (29), we may obtain the following equation:

$$\left(-\gamma\cos\alpha\right)^{-1}\sigma_c^{(B-1)/B}A^{-1/B}\left(M_1-\gamma b\cos\alpha\right)^{1/B}+N_1=0 \tag{35}$$

It should be noted that the simplified Eq. (35) is an implicit equation that includes only unknown parameters d_1 and θ_1 after M_1 and N_1 in Eqs. (33) and (34) are substituted into Eq. (35).

Similarly, according to the geometric relationships corresponding to failure curve $f_2(x)$ on the right shown in Fig. 1, we may obtain constants M_2 and N_2

$$M_2=\sigma_c A^{1/(1-B)}B^{B/(1-B)}\tan^{B/(1-B)}\theta_2+\gamma d_2\cos\alpha\cdot\cos\left(\beta-\alpha\right) \tag{36}$$

$$N_2=\frac{H}{\left(1+\tan\alpha\cdot\tan\beta\right)\cos\alpha}-d_2\sin\left(\beta-\alpha\right)+\left(\gamma\cos\alpha\right)^{-1}\sigma_c A^{1/(1-B)}B^{1/(1-B)}\tan^{1/(1-B)}\theta_2 \tag{37}$$

We may also obtain another implicit equation that includes only unknown parameters d_2 and θ_2

$$-\sigma_c^{(B-1)/B}A^{-1/B}\left(\gamma\cos\alpha\right)^{-1}\left(M_2-\gamma b\cos\alpha\right)^{1/B}+N_2=0 \tag{38}$$

On this basis, substitute Eqs. (25) and (26) into Eq. (18).

After integration and rearrangement, we may obtain the pullout capacity of the inclined strip anchor plate in the limit state

$$\begin{aligned}
P_u = &\left[d_1\cos(\beta-\alpha)-b\right](\sigma_t-\gamma N_1\cos\alpha)+\\
&\sigma_c^{(B-1)/B}A^{-1/B}(-\gamma\cos\alpha)^{-1}\cdot\\
&\frac{1}{1+B}\left\{\frac{\left[M_1-\gamma d_1\cos\alpha\cdot\cos(\beta-\alpha)\right]^{(B+1)/B}}{(M_1-\gamma b\cos\alpha)^{(B+1)/B}}-\right\}+\\
&\left[d_2\cos(\beta-\alpha)-b\right](\sigma_t-\gamma N_2\cos\alpha)+\\
&\sigma_c^{(B-1)/B}A^{-1/B}(-\gamma\cos\alpha)^{-1}\cdot\\
&\frac{1}{1+B}\left\{\frac{\left[M_2-\gamma d_2\cos\alpha\cdot\cos(\beta-\alpha)\right]^{(B+1)/B}}{(M_2-\gamma b\cos\alpha)^{(B+1)/B}}-\right\}+\\
&\left[\begin{array}{l}\dfrac{H(d_1+d_2)\cos(\beta-\alpha)}{(1+\tan\alpha\cdot\tan\beta)\cos\alpha}+\\ \dfrac{1}{4}\left(d_1^2-d_2^2\right)\sin 2(\beta-\alpha)\end{array}\right]\cdot\gamma\cos\alpha+\\
&q(d_1+d_2)\cos(\beta-\alpha)
\end{aligned} \tag{39}$$

where, constants M_1, N_1, M_2 and N_2 can be obtained by Eqs. (33) and (34) and Eqs. (36) and (37).

After simplification, the P_u expression in Eq. (39) contains only four unknown parameters d_1, d_2, θ_1 and θ_2. In addition, parameters d_1 and θ_1 should satisfy the implicit equation in Eq. (35), and parameters d_2 and θ_2 should satisfy the implicit equation in Eq. (38). In order to obtain the optimal upper bound solution, the minimum value of P_u should be sought. This is a typical constrained optimization problem. However, as the objective function P_u in Eq. (39) contains a large number of unknown parameters, and the constraint conditions in Eqs. (35) and (38) are implicit equations, it is very complex to solve. In order to solve this problem, this paper employed the nonlinear optimization solution function in the Lingo software to calculate the minimum value of P_u through programming, and to determine the corresponding failure range.

5. Results and discussion

Based on the above upper bound analysis, this paper proposed a theoretical prediction method for the pullout capacity of an inclined shallow anchor plate embedded in sloping rock ground. It should be noted that the above derivation process is performed on the basis of the Hoek-Brown failure criterion defined by normal stress σ_n and shear stress τ_n. However, in engineering practice, the design, construction and scientific research personnel may be more familiar with the Hoek-Brown failure criterion (Hoek and Broen 1997, Hoek and Marinos 2007, Hoek and Broen 2019, Zhu *et al.* 2013) defined by principal stress, asshown in Eq. (40). For example, currently, the built-in Hoek-Brown constitutive model in the FLAC-3D software is defined in the form of Eq. (40). In Eq. (40), rock strength parameters such as m_b, s and a are more commonly used.

They are obviously different from the rock parameters in Eq. (1). Thus, in order to better guide engineering application, this section adopts the more commonly used Hoek-Brown strength parameters in practice to investigate the influence laws of different factors on the anchor plate's pullout capacity and failure range.

$$\sigma_1=\sigma_3+\sigma_c\left(m_b\frac{\sigma_3}{\sigma_c}+s\right)^a \tag{40}$$

where, σ_1 is the maximum principal stress; σ_3 is the minimum principal stress; σ_c is rock compressive strength; m_b, s and a are dimensionless parameters related to rock properties, which can be calculated by the following equations.

$$\begin{cases} m_b=m_i\exp\left(\dfrac{GSI-100}{28-14D}\right)\\ s=\exp\left(\dfrac{GSI-100}{9-3D}\right)\\ a=\dfrac{1}{2}+\dfrac{1}{6}\left(e^{-\frac{GSI}{15}}-e^{-\frac{20}{3}}\right)\end{cases} \tag{41}$$

where, GSI is a geological strength index reflecting the rock quality grade; m_i is an empirical parameter reflecting the degree of rock hardness; its value ranges from 0.001 to 25; D is the coefficient reflecting the degree of external disturbance for the rock mass; its value ranges from 0 to 1. Parameters such as GSI, m_i and D can be determined by site surveys or laboratory tests.

In fact, for the same type of rock mass, the Hoek-Brown failure criterion defined by normal stress σ_n and shear stress τ_n. should be equivalent to that defined by principal stresses σ_1 and σ_3. That is, there must be a certain equivalent transformation relationship between rock strength parameters in Eq. (1) and those in Eq. (40). Specific to this problem, we can refer to the methods proposed by Gao et al. (2011) and Zuo and Shen (2020). The corresponding normal stress σ_n, shear stress τ_n., principal stress σ_1 and principal stress σ_3 in the case of rock failure should satisfy the following relations

$$\sigma_n=\frac{\sigma_1+\sigma_3}{2}-\frac{\sigma_1-\sigma_3}{2}\left(\frac{d\sigma_1/d\sigma_3-1}{d\sigma_1/d\sigma_3+1}\right) \tag{42}$$

$$\tau_n=(\sigma_1-\sigma_3)\frac{\sqrt{d\sigma_1/d\sigma_3}}{d\sigma_1/d\sigma_3+1} \tag{43}$$

where, according to Eq. (40), $d\sigma_1/d\sigma_3$ can be expressed as

$$\frac{d\sigma_1}{d\sigma_3}=1+am_b\left(\frac{m_b\sigma_3}{\sigma_c}+s\right)^{a-1} \tag{44}$$

At this time, if we know the Hoek-Brown failure criterion expression in the form of $\sigma_1-\sigma_3$ in Eq. (40), we may determine the value of any point (σ_1, σ_3) on the strength envelope curve; then, by using Eqs. (42)-(44), we may obtain the corresponding (σ_n, τ_n) value of any(σ_1, σ_3). On this basis, by fitting the series of (σ_n, τ_n) values by Eq. (1),

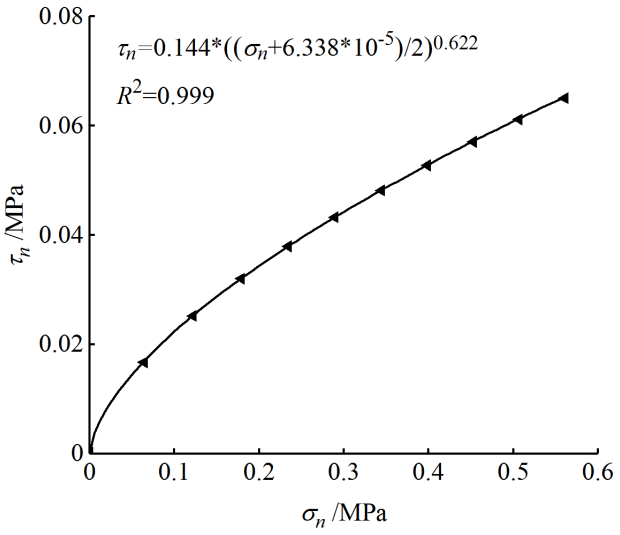

Fig. 2 Fitting curve of σ_n - τ_n

we may obtain the Hoek-Brown criterion expression defined by normal stress σ_n and shear stress τ_n. Then, the above two forms of Hoek-Brown strength parameters can be transformed. Taking parameters GSI=20, m_i=8, D=0.8 and σ_c = 2MPa as an example, Fig. 2 shows the strength envelope curve after fitting by Eq. (1). As can be seen from Fig. 2, the fitting precision of the series of (σ_n , τ_n) values obtained from Eqs. (42) and (43) is high, and the correlation coefficient is close to 1; this also shows the validity of the above parameter transformation method.

5.1 Influence of different mechanical parameters on ultimate pullout capacity of anchor plate

On this basis, by utilizing the above parameter transformation method, Fig. 3 shows the variation curves of the anchor plate's ultimate pullout capacities corresponding to different embedment depth/width ratio H/2b, anchor plate inclination α and ground inclination β. Where, the anchor plate's width is 2 m; the following rock strength parameters are adopted for calculation: GSI= 20, D = 0.8, m_i =8, σ_c = 2 MPa and γ = 20 kN/m^3, ground surface load q = 0 kPa.

According to Figs. 3(a)-3(c), as the embedment depth/width ratio $H/2b$ of the anchor plate increases, the corresponding ultimate pullout capacity increases significantly. For example, when the anchor plate inclination and ground inclination are constant, the ultimate pullout capacity with the embedment depth of 6 m is about 4 times that with the embedment depth of 2 m. Meanwhile, the ground inclination and the anchor plate inclination also have a significant influence on the ultimate pullout capacity.

When the ground inclination is constant, the ultimate pullout capacity decreases with the increase of the anchor plate inclination. When the anchor plate inclination is small, the ultimate pullout capacity increases with the increase of the ground inclination. When the anchor plate inclination exceeds a certain value, the ultimate pullout capacity decreases with the increase of the ground inclination.

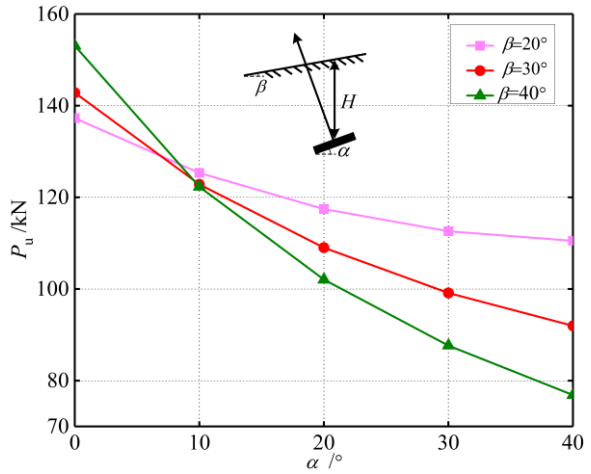

(a) $H/2b$ = 1

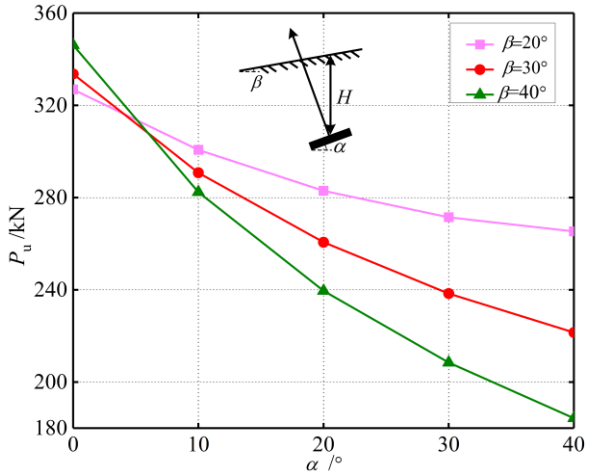

(b) $H/2b$ = 2

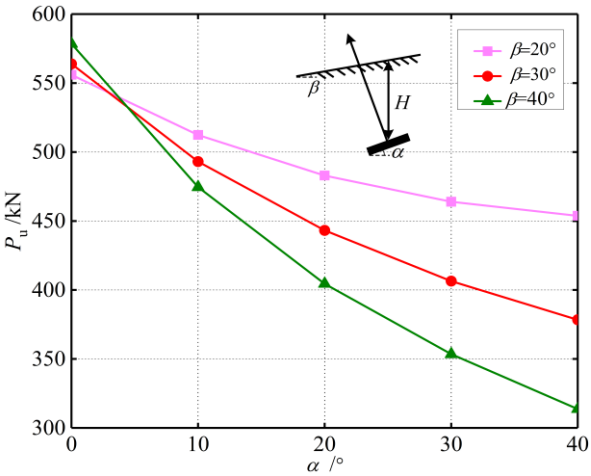

(c) $H/2b$ = 3

Fig. 3 Ultimate pullout capacities of anchor plates under different embedment depth/width ratios: (a) $H/2b$ = 1, (b) $H/2b$ = 2 and (c) $H/2b$ = 3

Therefore, in practical engineering, when the anchor plate's width is constant, increasing the embedment depth is one of the most effective ways to improve the pullout capacity. Moreover, during design of the anchor plate foundation, the influence of factors such as ground

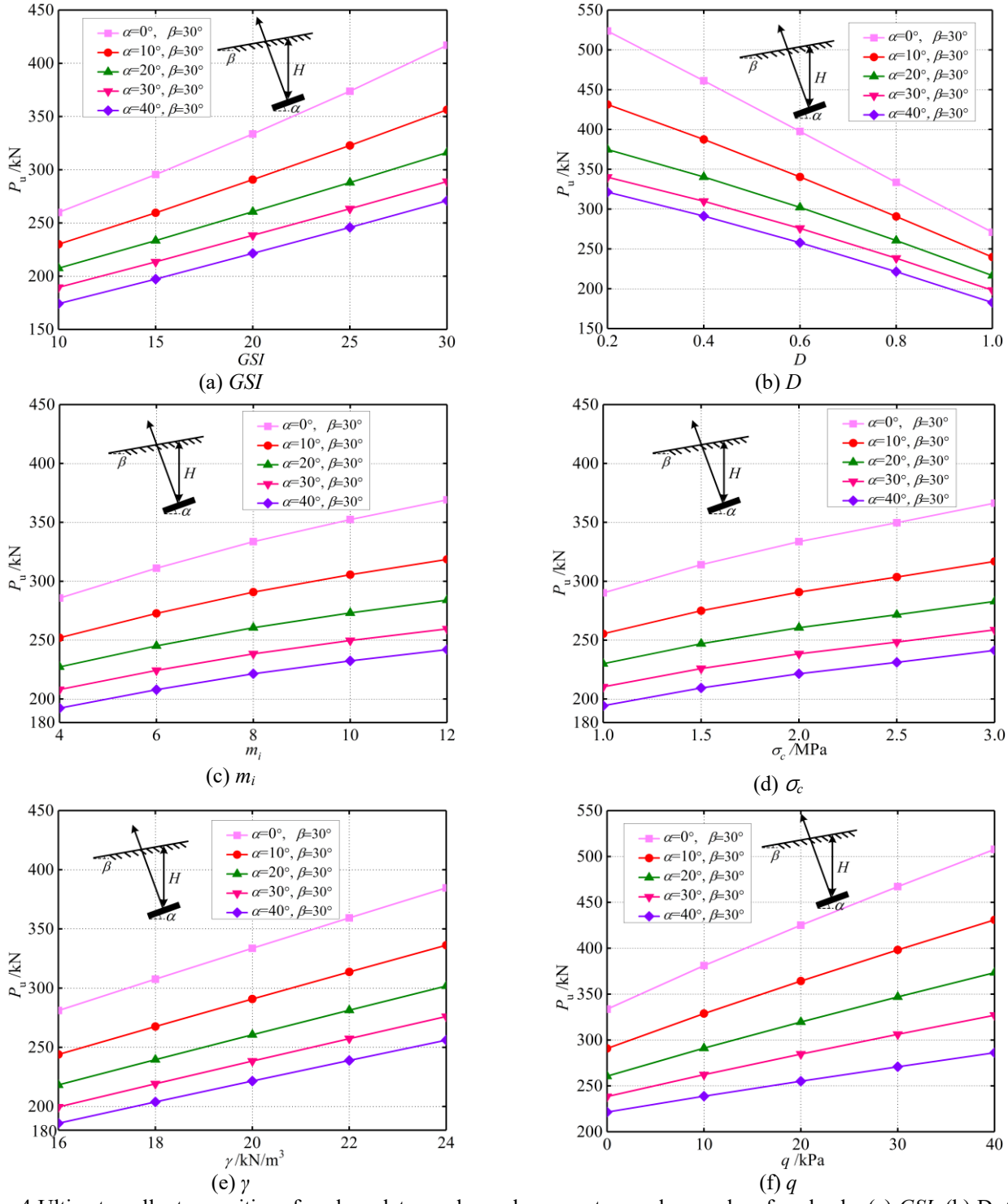

(a) *GSI* (b) *D*

(c) m_i (d) σ_c

(e) γ (f) q

Fig. 4 Ultimate pullout capacities of anchor plates under rock parameters and ground surface loads: (a) *GSI*; (b) D, (c) m_i, (d) σ_c, (e) γ and (f) q

inclination and anchor plate inclination should be considered comprehensively, and the optimal layout angle of anchor plate should be selected on the basis of the actual ground inclination, so as to obtain better pullout capacity.

Further, when anchor plate's embedment depth/width ratio $H/2b = 2$, ground inclination $\beta = 30°$ and anchor plate inclination $0 \sim 40°$, Fig. 4 shows the variation curves of the anchor plate's ultimate pullout capacities corresponding to different Hoek-Brown strength parameters and ground surface loads. Where, the following rock parameters are adopted for calculation: GSI = 10 ~ 30, D =0.2~1, $m_i = 4 \sim 12$, $\sigma_c = 1$~3MPa, $\gamma = 16 \sim 24 \text{kN/m}^3$ and ground surface load q = 0~40 kPa. When one of the parameters changes, the rest of the parameters remain constant.

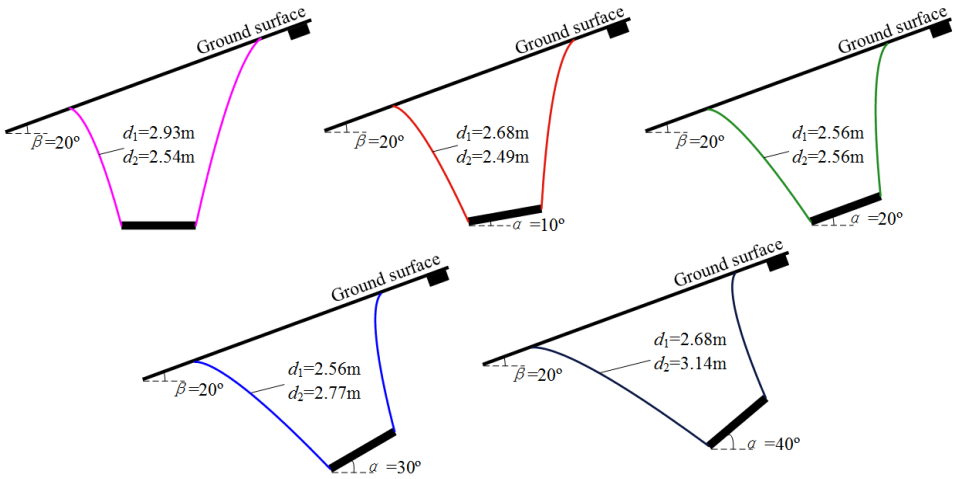

(a) $\beta = 20°$

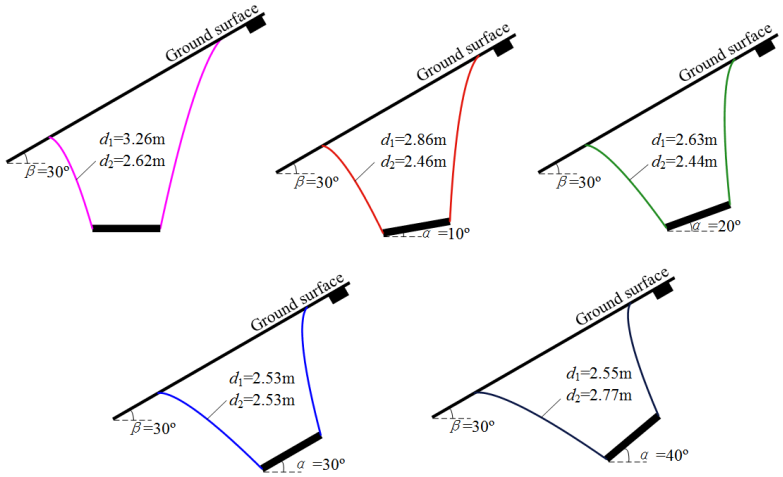

(b) $\beta = 30°$

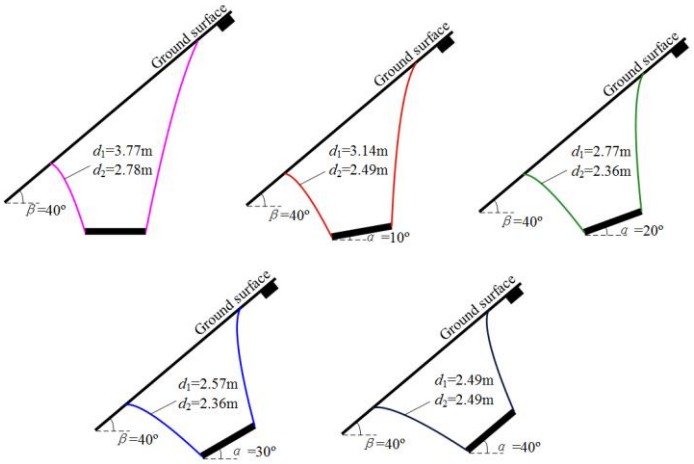

(c) $\beta = 40°$

Fig. 5 Rock failure surfaces under different ground inclinations and anchor plate inclinations: (a) $\beta = 20°$, (b) $\beta = 30°$ and (c) $\beta = 40°$

According to Figs. 4(a)-4(f), with the increase of the anchor plate inclination, the ultimate pullout capacity also tends to decrease. When Hoek-Brown strength parameters GSI, m_i and σ_c increase, the overall quality of the rock mass increases, and the corresponding ultimate pullout capacity increases. On the contrary, when the rock disturbance coefficient D increases, the external disturbance to the rock mass intensifies, and the rock quality tends to decrease; the corresponding ultimate pullout capacity decreases. Moreover, the geological strength index GSI and disturbance coefficient D have a significant influence on the anchor plate's ultimate pullout capacity. For example,

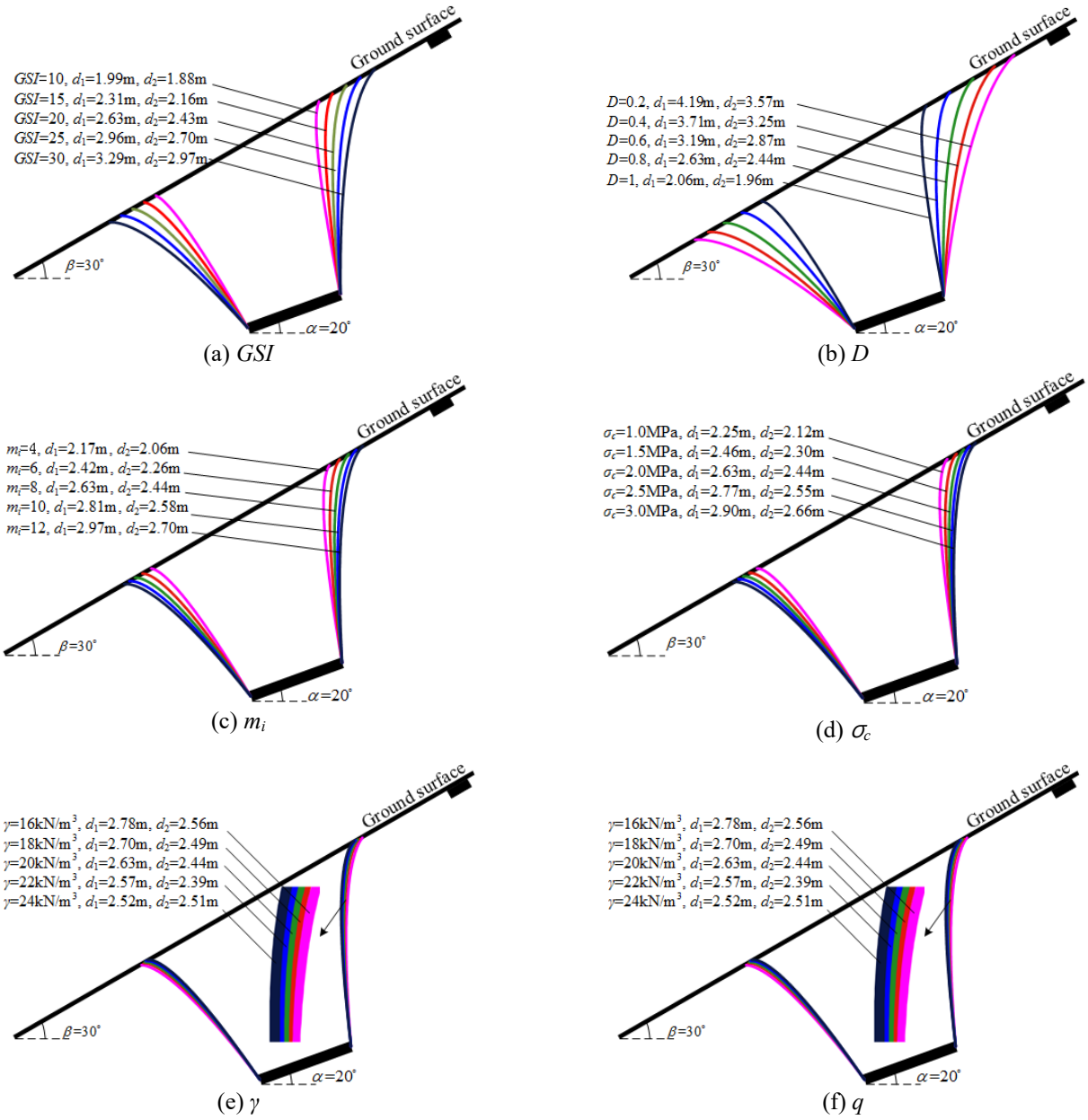

Fig. 6 Rock failure surfaces under different rock parameters and ground surface loads: (a) *GSI*; (b) D, (c) m_i, (d) σ_c, (e) γ and (f) q

when the anchor plate inclination is 0º and the ground inclination is 30º, the ultimate pullout capacity corresponding to D = 0.2 is about 2 times that corresponding to D = 0.1. Besides, when the rock unit weight γ and ground surface load q increase, the resistance to the anchor plate's uplift failure increases, and the corresponding ultimate pullout capacity tends to increase.

5.2 Influence of different mechanical parameters on shape of rock failure surface

In order to investigate the influence of different parameters on the shape of the rock failure surfaces above the inclined anchor plate, here we set anchor plate's width b = 2 m and embedment depth/width ratio $H/2b$ = 2. Fig. 5 shows the rock failure curves corresponding to different ground inclinations and anchor plate inclinations. The failure width values at the ground surface are also marked in Fig. 5. Where, the following rock parameters are adopted for calculation: *GSI* =20, D=0.8, m_i = 8, σ_c = *2* MPa, γ = *20* Kn/m^3 and ground surface load q = 0 kPa.

As can be seen from Figs. 5 (a)-5(c), because both the ground surface and the anchor plate have a certain inclination, the rock failure range above the anchor plate shows obvious asymmetry. On the whole, as the anchor plate inclination increases, the rock failure range tends to incline downward along the slope. Specifically, when the anchor plate inclination is less than the ground inclination, the failure width on the left is less than that on the right at

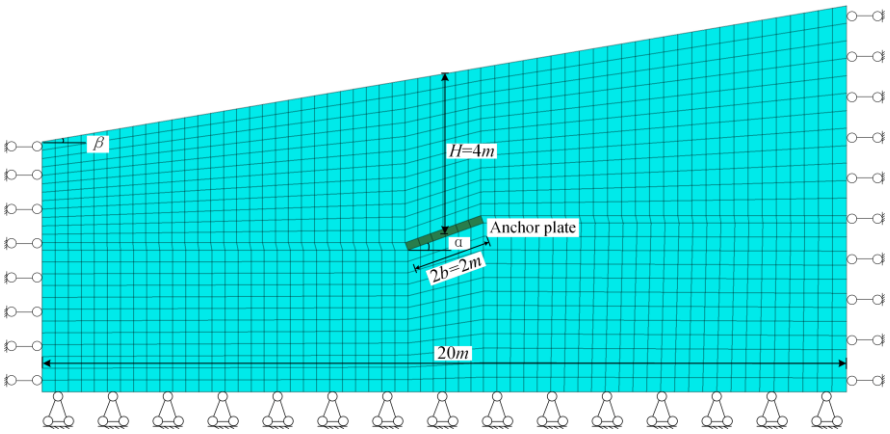

Fig. 7 Numerical simulation model for an inclined anchor plate

Table 1 Parameters for numerical simulation under different schemes

Item	α/°	β/°	b/m	H/m	σ_{ci}/MPa	GSI	D	m_i
1	10	10	1	4	2	20	0.8	8
2	20	10	1	4	2	20	0.8	8
3	30	10	1	4	2	20	0.8	8
4	10	20	1	4	2	20	0.8	8
5	20	20	1	4	2	20	0.8	8
6	30	20	1	4	2	20	0.8	8

the ground surface; when the anchor plate inclination is greater than the ground inclination, the failure width on the left is greater than that on the right; when the ground inclination is the same as the anchor plate inclination, the rock failure width on the left is equal to that on the right.

Further, taking the embedment depth/width ratio $H/2b$=2, anchor plate inclination α = 20º and the ground inclination β = 30º as an example, Fig. 6 shows the rock failure curves corresponding to different rock parameters GSI, D, m_i, σ_c, γ and ground surface load q.

As can be seen from Figs. 6(a)-6(f), when other parameters remain constant, as the geological strength index GSI, parameter m_i and rock compressive strength σ_c increase, the rock failure range above the anchor plate tends to increase. Conversely, as the disturbance coefficient D, ground surface load q and rock unit weight γ increase, the rock failure range tends to decrease. Where, the disturbance coefficient D has the most significant influence on the failure range. Therefore, during engineering design and construction, the disturbance damage (Wang *et al.* 2019, Wang *et al*. 2020) caused by external factors to the rock mass should be reduced as much as possible, so as to improve the stability and pullout capacity of the anchor plate foundation.

6. Comparison with numerical simulation results

To further verify the correctness of the proposed theoretical method in this paper, this section uses the finite difference software FLAC-3D to carry out numerical simulation for the pullout process of inclined anchor plates in sloping ground under six schemes. Fig. 7 shows the numerical simulation model. Specifically, horizontal and vertical displacements are fixed at the bottom boundary of the model; horizontal displacement is fixed at the front, rear, left and right boundaries; the top surface is a free boundary. In the model, the rock mass is simulated by the built-in Hoek-Brown constitutive model of the FLAC-3D software. Table 1 lists the specific parameters corresponding to the six schemes. Meanwhile, during modeling, common nodes are set between the anchor plate and the rock mass to simulate the interaction between them.

It should be noted that the numerical simulation in this section is just to validate the effectiveness of the proposed method in this paper. The rock mass around the anchor plate is assumed to be homogenous, and the installation process is also ignored, in order to obtain convincing results under the same conditions. Specifically, in the numerical simulation, after the initial geostress field that is applied to the model achieves a balance, taking the center of the anchor plate as the control point, the displacement load perpendicular to the surface of the anchor plate is applied to simulate the pullout failure process. The applied displacement load is 10^{-5} m/time step. Fig. 8 shows the process curves between the pullout load and the pullout displacement under the above six simulation schemes.

As can be seen from Fig. 8, in the pullout process, as the displacement increases, the pullout load that the anchor plate can bear increases rapidly until it reaches the peak

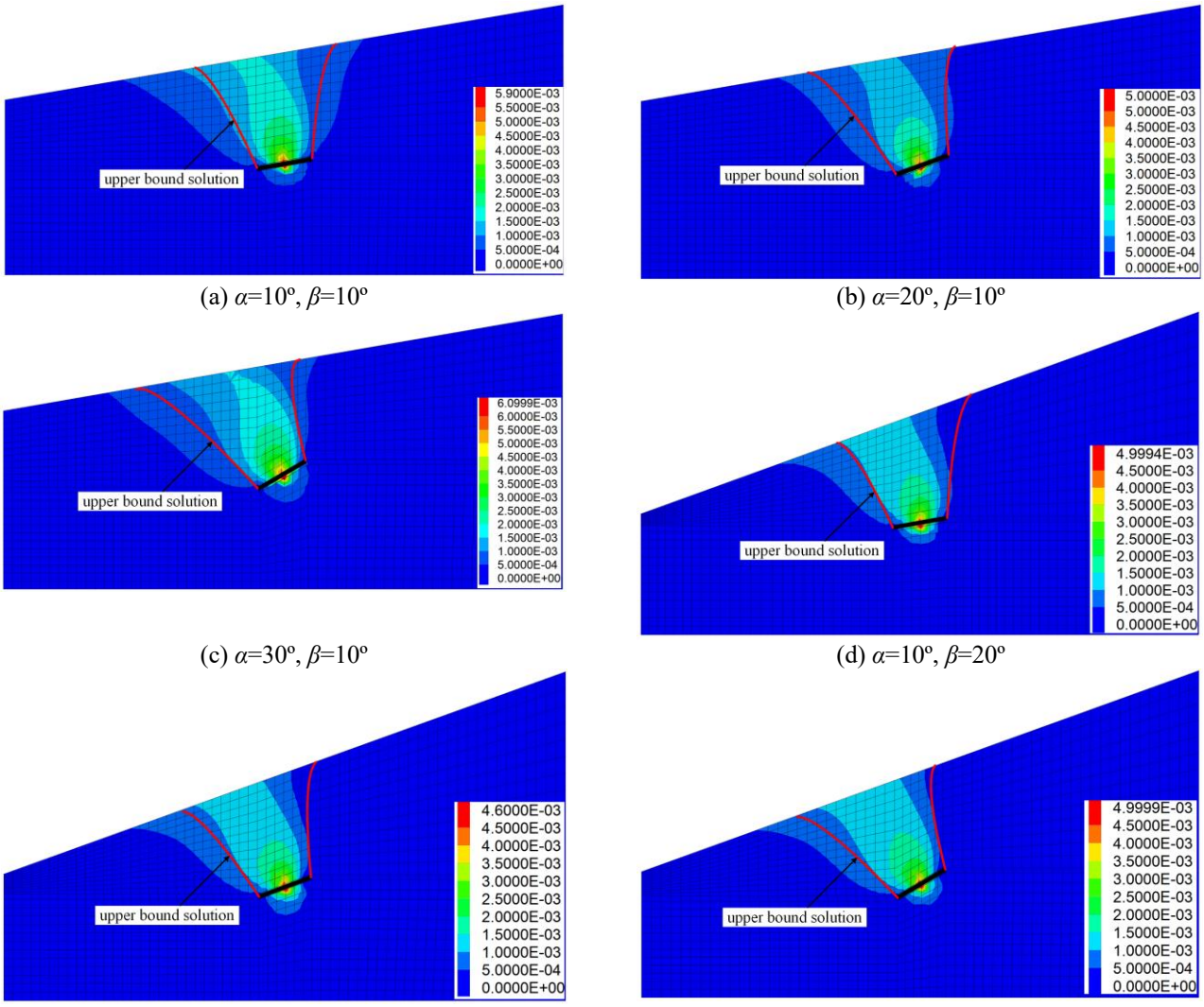

(a) α=10º, β=10º (b) α=20º, β=10º

(c) α=30º, β=10º (d) α=10º, β=20º

(e) α=20º, β=20º (f) α=30º, β=20º

Fig. 9 Contours of displacement magnitude at critical failure state under different schemes: (a) α=10º, β=10º, (b) α=20º, β=10º, (c) α=30º, β=10º, (d) α=10º, β=20º, (e) α=20º, β=20º and (f) α=30º, β=20º

Table 2 Comparison of ultimate pullout capacities obtained by the upper bound solution and the numerical simulation

Item	α/º	β/º	Upper bound solution /kN	Numerical simulation result /kN	Result difference
1	10	10	312.23	325.43	4.1%
2	20	10	307.87	321.94	4.4%
3	30	10	310.29	316.49	2%
4	10	20	314.62	300.69	4.4%
5	20	20	282.95	291.55	2.9%
6	30	20	271.47	280.7	3.3%

point. After the peak point, due to the monolithic failure of the rock mass above the anchor plate, as the pullout displacement increases, the pullout load decreases, and then gradually shows a slow downward trend. Further, the peak point is regarded as the critical failure state, and the corresponding peak pullout load is taken as the ultimate pullout capacity of the anchor plate. Table 2 lists the numerical simulation results corresponding to the six schemes and the upper bound solutions obtained by the proposed method in this paper. As can be seen from Fig. 2, all the upper bound solutions are close to the numerical simulation results, and the maximum difference is not more than 4.4%. For example, when $\alpha = 20^{\circ}$ and $\beta = 20^{\circ}$, the numerical simulation result for the anchor plate's ultimate pullout capacity is 291.55 kN, while the upper bound solution is 282.95 kN; the difference is only 2%, which also verifies the validity of the proposed method in this paper.

In addition, Figs. 9 and 10 show the contours of displacement magnitude and the contours of shear strain rate corresponding to the critical failure states of the anchor plates. The rock failure curves calculated by the upper bound method are also shown in Figs. 9 and 10 for comparison. As can be seen from Figs. 9 and 10, due to the existence of a certain inclination between the ground surface and the anchor plate, the numerical simulation result

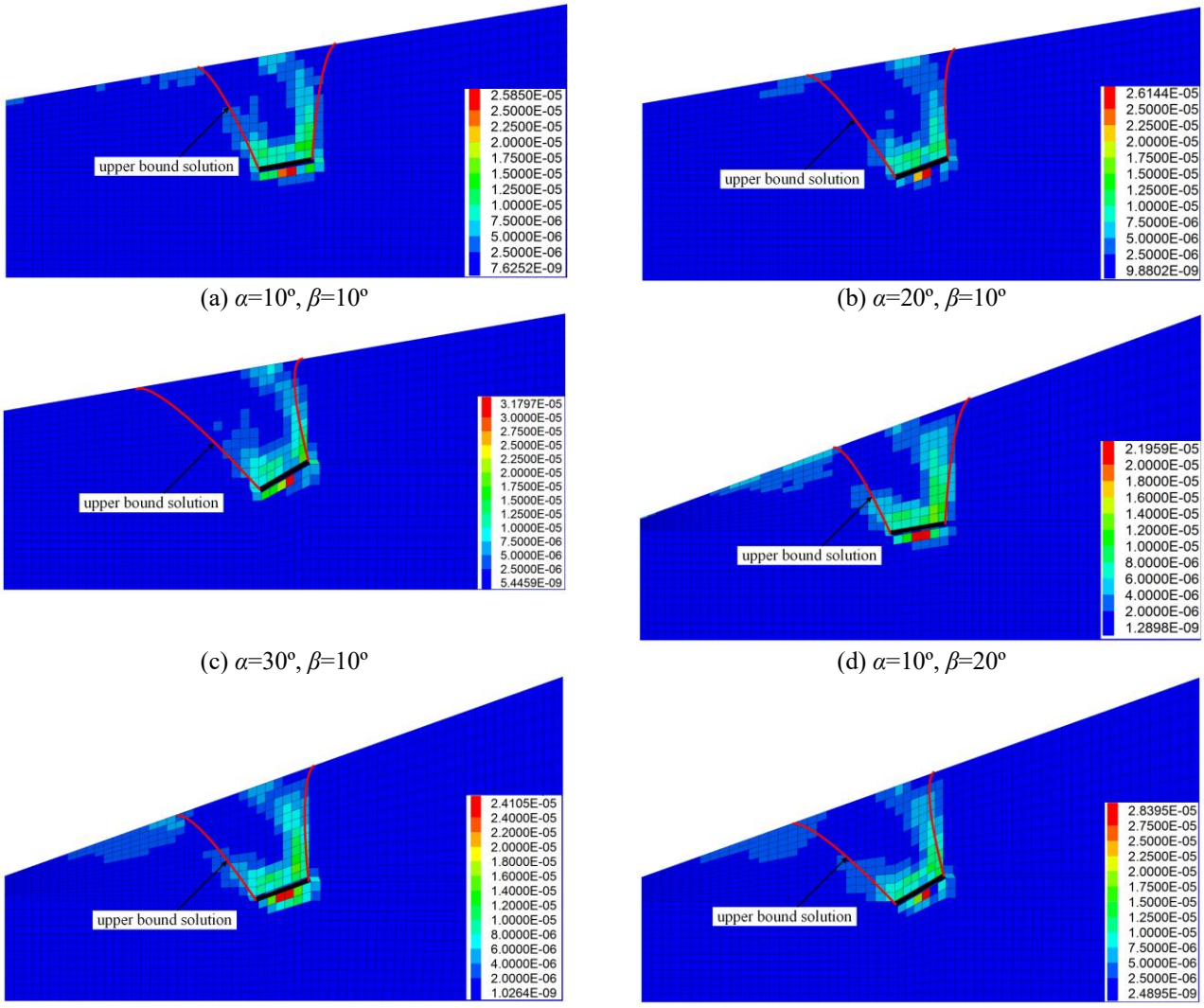

(a) α=10º, β=10º (b) α=20º, β=10º

(c) α=30º, β=10º (d) α=10º, β=20º

(e) α=20º, β=20º (f) α=30º, β=20º

Fig. 10 Contours of shear strain rate at critical failure state under different schemes: (a) α=10º, β=10º, (b) α=20º, β=10º, (c) α=30º, β=10º, (d) α=10º, β=20º, (e) α=20º, β=20º and (f) α=30º, β=20º

of each scheme shows that the rock failure range above the anchor plate is approximately in asymmetric trumpet shape that is "wide at the top and narrow at the bottom." Moreover, as the slope inclination increases, the rock failure range tends to incline downward along the slope, which is consistent with the failure characteristics described in section 5.2. The rock failure range obtained by the upper bound method is roughly consistent with that calculated by numerical simulation, which further verifies the validity of the proposed method in this paper.

7. Conclusions

(1) Focusing on the shallow-buried inclined strip anchor plates in sloping rock ground, this paper proposed an asymmetrical curve failure mechanism for the rock masses above the anchor plates. Then, by using the Hoek-Brown failure criterion and upper bound method, this paper deduced the theoretical analytical solutions for the anchor plate's ultimate pullout capacity and the rock failure surface in the limit state. On this basis, a Hoek-Brown strength-parameter equivalent transformation method was employed to systematically investigate the influence laws of various parameters on the ultimate pullout capacity and the rock failure range. Finally, the numerical simulation was carried out for the pullout process of an inclined anchor plate under six schemes to further validate the proposed method in this paper.

(2) The embedment depth, ground inclination, anchor plate inclination, geological strength index *GSI* and disturbance coefficient *D* are significant factors affecting the anchor plate's ultimate pullout capacity; we should attach importance to them in engineering design and construction. Specifically, when the ground is inclined, the ultimate pullout capacity tends to decrease with the increase of the anchor plate inclination, the optimum value for inclination angle of anchor plate is 0º; when the anchor plate inclination is over 10º, the optimum ground inclination is suggested to be no more than 20º. The anchor

plate's ultimate pullout capacity is positively correlated with Hoek-Brown strength parameters *GSI*, m_i and σ_c, rock unit weight γ and ground surface load q, but it is negatively correlated with rock disturbance coefficient D.

(3) For inclined anchor plates in sloping rock ground, the rock failure range above the anchor plate shows obvious asymmetry. On the whole, as the anchor plate inclination increases, the rock failure range tends to incline downward along the slope. Moreover, the rock failure range above the anchor plate is positively correlated with geological strength index *GSI*, parameter m_i and rock compressive strength σ_c, but it is negatively correlated with disturbance coefficient D, ground surface load q and rock unit weight γ.

Acknowledgements

Much of the work presented in this paper was supported by the National Natural Science Foundation of China (No. 52374093), Project funded by China Postdoctoral Science Foundation (No. 2022M711314), Shandong Provincial Natural Science Foundation (No. ZR2022ME088), and a Project of Shandong Province Higher Educational Science and Technology Program (J16LG04). The authors also would like to express appreciation to the reviewers for their valuable comments and suggestions, which improved the paper much.

References

Bhattacharya, P. and Kumar, J. (2016), "Uplift capacity of anchors in layered sand using finite-element limit analysis: Formulation and results", *Int. J. Geomech*., **16**(3), 04015078. https://doi.org/10.1061/(ASCE)GM.1943-5622.0000560.

Bhattacharya, P. (2016), "Pullout capacity of strip plate anchor in cohesive sloping ground under undrained condition", *Comput. Geotech*., **78**, 134-143.

Chen, W.F. (1975), Limit analysis and soil plasticity. Elsevier, Amsterdam.

Choudhary, A.K. and Dash, S.K. (2017), "Load-carrying mechanism of vertical plate anchors in sand", *Int. J. Geomech*., **17**(5), 04016116. https://doi.org/10.1061/(ASCE)GM.1943-5622.00008.

Cerfontaine, B., Knappett, J.A., Brown, M.J. and Bradshaw , A.S. (2019), "Effect of soil deformability on the failure mechanism of shallow plate or screw anchors in sand", *Comput. Geotech.*. **109**, 34-45. https://doi.org/10.1016/j.compgeo.2019.01.007.

Gao, Y.T., Yang, Z.M., Cheng, Z.Q., Jiang, Y. and Ren, Y. (2011), "Limit analysis of tunnel collapse according to the Hoek-Brown criterion and bolt parameter research", *Arabian J. Sci. Eng*., **44**(10), 8171-8180. https://doi.org/10.1007/s13369-019-03731-y.

Ganesh, R. (2020), "Vertical uplift resistance of close-spaced shallow rectangular group anchor plates embedded in sand", *Mar. Georesour. Geotechnol.,* **38**(9), 1070-1081. https://doi.org/10.1080/1064119X.2019.1650403.

Hoek, E. and Broen, E.T. (1997), "Practical estimates of rock mass strength", *Int. J. Rock Mech. Min. Sci*., **34**(8), 1165-1186. https://doi.org/10.1016/S1365-1609(97)80069-X.

Hoek, E. and Marinos, P. (2007), "A brief history of the development of the Hoek-Brown failure criterion", *Soils Rocks*, (2).

Hao, D.X., Fu, S.N. and Chen, R. (2014), "Numerical analysis of uplift capacity of circular plate anchor in sand", **19**, 18947-18961.

Hanna, A., Foriero, A. and Ayadat, T. (2015), "Pullout capacity of inclined shallow single anchor plate in sand", *Indian Geotech. J.,* **45**(1), 110-120. https://doi.org/10.1007/s40098-014-0113-7.

Han, C., Wang, D., Gaudin, C., O'Loughlin, C.D. and Cassidy, M.J. (2016), "Behaviour of vertically loaded plate anchors under sustained uplift", *Geotechnique*, **66**(8), 681-693. https://doi.org/10.1680/jgeot.15.P.232.

Hoek, E. and Broen, E.T. (2019), "The Hoek-Brown failure criterion and GSI-2018 edition", *J. Rock Mech. Geotech. Eng*., **11**(3), 445-463. https://doi.org/10.1016/j.jrmge.2018.08.001.

Hu, W., Meng, J.W., Yao, C. And Lwi, Y. (2020), "A method for calculating vertical pullout ultimate bearing capacity of shallow circular anchor plate", *Rock Soil Mech*., **41**(9), 3049-3055.

Hu, S., Zhao, L., Tan, Y., Yang, F., Wang, Z. And Zhao, Z. (2021), "Variation analysis of uplift bearing characteristics of strip anchor plate in nonhomogeneous materials", *Int. J. Geomech*., **21**(4), 04021037. https://doi.org/10.1061/(ASCE)GM.1943-5622.0001974.

Hu, S., Zhao, L., Tan, Y., Luo, Y. and Zeng, Z. (2022), "Three-dimensional upper-bound limit analysis of ultimate pullout capacity of anchor plates using variation method", *Int. J. Numer. Anal. Method. Geomech*., **46**(7), 1356-1379. https://doi.org/10.1002/nag.3349.

.Kumar, J. and Kouzer, K.M. (2008), "Vertical uplift capacity of horizontal anchors using upper bound limit analysis and finite elements", *Can. Geotech. J.,* **45**(5), 698-704. https://doi.org/10.1139/T08-005.

Khatri, V.N. and Kumar, J. (2009), "Vertical uplift resistance of circular plate anchors in clays under undrained condition", *Compu. Geotech.*, **36**(8), 1352-1359. https://doi.org/10.1016/j.compgeo.2009.06.008.

Perazzelli, P. and Anagnostou, G. (2017), "Uplift resistance of strip anchors in cohesive frictional mediums of limited tensile strength", *Int. J. Geomech.,* **17**(9), 04017042. https://doi.org/10.1061/(ASCE)GM.1943-5622.0000901.

Rokonuzzaman, M. and Sakai, T. (2012), "Model tests and 3D finite element simulations of uplift resistance of shallow rectangular anchor foundations", *Int. J. Geomech.*, **12**(2), 105-112. https://doi.org/10.1061/(ASCE)GM.1943-5622.00001.

Roy, A. (2020), "Numerical and experimental investigation of plate anchor capacity in sand", *The University of Western Australia.*

Wang, H.T., Li, S.C., Wang, Q., Miao, S.J. and Jiang, B. (2014), "Limit analysis of ultimate pullout capacity of shallow horizontal strip anchor plate based on nonlinear failure criterion", *Eng. Mech*., **31**(2), 131-138. https://doi.org/10.6052/j.issn.1000-4750.2012.09.0699.

Wang, Q., Gao, H.K., Yu, H.C., Jiang, B. and Liu, B.H. (2019), "Method for measuring rock mass characteristics and evaluating the grouting-reinforced effect based on digital drilling", *Rock Mech. Rock Eng*., **52**, 841-851.

Wang, H.T., Wang, L.G., Li, S.C., Wang, Q., Liu, P. and Li, X. (2019), "Roof collapse mechanisms for a shallow tunnel in two-layer rock strata incorporating the influence of groundwater", *Eng. Fail. Anal*., **98**, 215-227. https://doi.org/10.1016/j.engfailanal.2019.01.062.

Wang, Q., Gao, H.K., Jiang, Z.H., Li, S.C. and Jiang, B. (2020), "Development and application of a surrounding rock digital drilling test system of underground engineering", *Chinese J. Rock Mech. Eng.*, **39**(2), 301-310.

Wang, H.T., Liu, L.Y., Li, S.C., Wang, Q., Li, W. and Meng, Q. (2021), "An upper bound design method for roof bolting support in roadways with top coal", *Arabian J. Geosci*., **14**(9),

1-12. https://doi.org/10.1007/s12517-021-06660-z.

Yang, M.H., Ai, Z.C. and Deng, B. (2020), "Experimental and analytical study on uplift loading capacity of strip plate anchors near sand slope", *Int. J. Geomech.*, **20**(1), 04019136. https://doi.org/10.1061/(ASCE)GM.1943-5622.000152.

Zhang, R. and Yang, X.L. (2019), "Limit analysis of anchor trapdoor embedded in nonhomogeneous and nonlinear soils", *Int. J. Geomech*., **19**(8), 04019089. https://doi.org/10.1061/(ASCE)GM.1943-5622.0001476.

Zhu, H.H., Zhang, Q. and Zhang, L.Y. (2013), "Review of research progresses and applications of Hoek-Brown strength criterion", *Chinese J. Rock Mech. Eng.,* **32**(10), 1945-1963.

Zhao, L.H., Tan, Y.G., Nie, Z.H., Yang, X.P. and Hu, S.H. (2018), "Variation analysis of ultimate pullout capacity of shallow horizontal strip anchor plate with 2-layer overlying soil based on nonlinear MC failure criterion", *J. Central South Univ.*, **25**(11), 2802-2818. https://doi.org/10.1007/s10706-022-02357-6

Zhao, L., Gong, X., Hu, S., Tan, Y. and Zhao, Z. (2022), "Effects of heterogeneity and nonlinearity on uplift characteristics of shallow horizontal anchor plates", *Geotech. Geol. Eng*., **41**, 1615-1634. https://doi.org/10.1007/s10706-022-02357-6.

Zuo, J. and Shen, J. (2020), The Hoek-Brown failure criterion-from theory to application. Singapore: Springer Nature Singapore Private Limited.

IC

List of symbols

τ_n	The shear stress at the rock failure surface
σ_n	The normal stress at the rock failure surface
σ_t	The tensile strength of the rock mass
σ_c	The compressive strength of the rock mass
A, B	The empirical coefficients related to rock-mass properties
v	The velocity vector within the velocity field
α	The inclination angle of strip anchor plate
β	The inclination angle of rock slope
$2b$	The width of strip anchor plate
P_u	The uplift load
q	The additional surface load
$f_1(x)$	The curve equation of the right failure surface above the anchor plate
$f_2(x)$	The curve equation of the left failure surface above the anchor plate
d_1	The failure width on the right side of the ground surface
d_2	The failure width on the left side of the ground surface
H	The vertical embedment depth of the anchor plate's center
F	The yield function of rock mass
Q	The plastic potential function
$\dot{\lambda}$	The plastic factor
$\dot{\varepsilon}_{ij}$	The plastic strain rate vector
σ_{ij}	The stress vector
$\dot{\varepsilon}_{n1}$	The plastic positive strain rate
$\dot{\gamma}_{n1}$	The plastic shear strain rate
W_1	The thickness of the thin layer at the rock failure surface on the right
$f_1'(x)$	The first derivative of $f_1(x)$
$\dot{D}_1$	The energy dissipation rate per unit volume at the right failure surface
$\dot{D}_2$	The energy dissipation rate per unit volume at the left failure surface
W_2	The thickness of the thin layer at the rock failure surface on the left
$\dot{W}_{i1}$	The internal energy dissipation rate generated at the right failure surface
$\dot{W}_{i2}$	The internal energy dissipation rate generated at the left failure surface
S_1	The total length of curve $f_1(x)$
S_2	The total length of curve $f_2(x)$
$\dot{W}_i$	The total internal energy dissipation rate
$\dot{W}_{\gamma 1}$	The work rate of rock weight on the right side above the anchor plate
$\dot{W}_{\gamma 2}$	The work rate of rock weight on the left side above the anchor plate
γ	The unit weight of rock mass
$\dot{W}_{\gamma}$	The total work rate of rock weight above the anchor plate
$\dot{W}_q$	The work rate of the ground surface load
$\dot{W}_P$	The work rate of the anchor plate's ultimate pullout capacity
$\Lambda_1[f_1(x), f_1'(x), x]$	The functional of $f_1(x)$
$\Lambda_2[f_2(x), f_2'(x), x]$	The functional of $f_2(x)$
M_1, N_1, M_2, N_2	The integration constants
θ_1	The angle between the right failure curve $f_1(x)$ and the ground surface
θ_2	The angle between the left failure curve $f_2(x)$ and the ground surface
σ_1	The maximum principal stress
σ_3	The minimum principal stress
m_b, s, a	The dimensionless parameters related to rock properties
GSI	The geological strength index reflecting the rock quality grade
m_i	The empirical parameter reflecting the degree of rock hardness
D	The coefficient reflecting the external disturbance degree for the rock mass